Time resolved spectra and energy transfer analysis of Nd^{3+}-Yb^{3+}-Er^{3+} triply-doped Ba-Al-metaphosphate glasses for an eye safe emission (1.54 μm)

Atul D. Sontakke, Kaushik Biswas, Ashis K. Mandal, K. Annapurna*
Glass Technology Laboratory, Central Glass and Ceramic Research Institute
(Council of Scientific and Industrial Research)
196, Raja S.C. Mullick Road, Kolkata 700032, India

Abstract

This paper reports on the development and systematic analysis of energy transfer mechanisms in Nd^{3+}-Yb^{3+}-Er^{3+} co-doped new series of barium-alumino-metaphosphate glasses. The time resolved fluorescence spectra of Nd^{3+} in triply doped Ba-Al-metaphosaphte glasses have revealed that, Yb^{3+} ions could function as quite efficient bridge for an energy transfer between Nd^{3+} and Er^{3+} ions. As a result, a fourfold emission enhancement at 1.54 μm of Er^{3+} ions has been achieved through an excitation of $^4F_{5/2}$ level of Nd^{3+} at 806 nm for the glass having 3 mol% Yb^{3+} with an energy transfer efficiency reaching up to 94%. Decay of donor (Nd^{3+}) ion fluorescence has been analyzed based on theoretical models such as Inokuti-Hirayama, Burshtein (migration) and Yokota-Tanimoto (diffusion) and corresponding energy transfer parameters have been discussed. Primarily, electrostatic dipole-dipole (s ~ 6) interactions are found to be responsible for the occurrence of energy transfer process in theses glasses.

Key words: Metaphosphate glasses, energy transfer, fluorescence, sensitized Er^{3+} emission.

* Corresponding author : Tel.: +91-33 2473 3469; Fax: +91-33 2473 0957
Email : glasslab42@hotmail.com (K. Annapurna)

Introduction

Sensitized emission occurrence from the lanthanide ions (Ln^{3+}) has attracted significant attention and importance. The energy transfer efficiency among donor-acceptor ions depends on overlapping of donor's emission with that of activator's absorption and their inter-ionic distances. Hence, heavily doped solid-state gain media including laser crystals, glasses and rare earth doped fibers have recently been considered more relevant for energy transfer luminescence studies. A great deal of work has been carried out in exploring the energy transfer amongst lanthanides ($RE^{3+} \rightarrow RE^{3+}$) as well as transition metal ions with lanthanides ($TM \rightarrow RE^{3+}$) ions in the visible (VIS) region [1-3]. The main interest of those works has been focused on rare earth ions like Eu^{3+}, Tb^{3+}, which could be sensitized by UV absorbing Ce^{3+}, Gd^{3+} ions for their potential use in lighting, display and dosimetric applications [4, 5]. With the emergence of laser diodes, the interest has been extended towards the NIR emitting ions like Pr^{3+}, Nd^{3+}, Tm^{3+}, Ho^{3+}, Er^{3+} and Yb^{3+} etc. NIR emission plays an important role in optical communications, biomedical applications and lasers [6, 7] such as Nd^{3+} based laser systems, which are well known for their high power applications [8]. However, for certain singly doped ions, like Yb^{3+} based lasers, various technical problems arise for high power operation; since the energy difference between excitation and emission is very small due to its two level configurations [9]. Some attempts have been made earlier in finding a suitable glass host so as to bring in a wider separation from the Stark components of lower energy states of Yb^{3+} resulting in with a quasi-three level system [10]. Yet another good solution to overcome this difficulty is to sensitize it with Nd^{3+} ion so as to achieve an efficient lasing at 980 nm from Yb^{3+} on exciting the Nd^{3+} ion with easily available high power 800nm

laser diode [11, 12]. Beside its lasing performance, Yb^{3+} serves as good sensitizer for several lanthanides (Pr^{3+}, Ho^{3+}, Tm^{3+}, Er^{3+} etc.) because of its high absorption and emission cross-section in combination with higher allowed doping concentrations. Its sensitization is based on either resonant energy transfer (RET) or phonon-assisted energy transfer (PAET) for improved NIR emission and energy transfer upconversion (ETU) for visible emissions from activator ions [13, 14]. Among these, Er^{3+} possesses special interest due to its NIR emission at eye safe wavelength (1.53 μm). In addition, it has been recognized as one of the most efficient rare earth ions to be used in optical communication and range finder applications since its emission coincides with the third communication/atmospheric window (1.525 – 1.565 μm) [15]. For Nd^{3+}-Yb^{3+} or Yb^{3+}-Er^{3+} systems, the energy transfer is more or less resonant since the emission of sensitizer overlaps with absorption of activator and such systems have been widely studied. However, very few reports are available on Nd^{3+} sensitization to Er^{3+} ions [16]. Moreover, in this system it was found that the spectral energy mismatch of 1150 cm^{-1} does exist between donor (Nd^{3+}) and acceptor (Er^{3+}) and hence phonon assisted energy transfer may be responsible for this process. Since Yb^{3+} ions can act as activators for Nd^{3+} and very efficient sensitizers for Er^{3+}, it can be expected to achieve improved energy transfer from Nd^{3+} to Er^{3+} in the presence of Yb^{3+} as bridging ions. An attempt has been made to examine the $Nd^{3+} \rightarrow Er^{3+}$ energy transfer with the presence and absence of Yb^{3+} ions in alkali free Barium-alumino-metaphosphate glass host.

Metaphosphate glasses are advantageous over silicate and other host glasses for their high rare earth ion doping concentration without considerable fluorescence

quenching along with possessing low melting temperature and several favorable spectroscopic properties including high emission cross-sections and longer fluorescence lifetime of active ions and hence have been used in the development of high power solid-state lasers [17]. Among them, sodium phosphate, barium phosphate, alumino-metaphosphate and potassium-alumino-metaphosphate glasses have been studied widely [18-21]. In addition to these several other metaphosphate glasses including Zn- or Pb-metaphosphate have also been investigated for their optical and spectroscopic properties in the presence of active ions [22]. However, to our knowledge, there are no reports so far on alkali free barium-alumino-metaphosphate glass system in the literature.

Hence, in the present work our main objective is to prepare a new series of alkali free barium-alumino-metaphosphate glasses containing mono, bi and tri rare earth ions (Nd^{3+}-Yb^{3+}-Er^{3+}) and to examine the intermediate Yb^{3+} ion influence on the sensitization efficiency of Nd^{3+} for NIR emission from Er^{3+} ions. The energy transfer mechanism between Nd^{3+} and Er^{3+} ions in the presence and absence of Yb^{3+} has been systematically analyzed from the measurement of photoluminescence spectra and the time resolved decay profiles of these new series of optical glass systems by employing theoretical models.

Experimental Study

The glasses in the following chemical compositions (in mole %) were developed by employing melt quenching method:

1. **BAP-Nd**: $11.60Al_2O_3$-20.73BaO-$55.54P_2O_5$-$6.72SiO_2$-$3.86B_2O_3$-$0.5Nb_2O_3$-$1.05Nd_2O_3$

2. **BAP-Er**: $11.60Al_2O_3$-$20.73BaO$-$55.54P_2O_5$-$6.72SiO_2$-$3.86B_2O_3$-$0.5Nb_2O_3$-$1.05Er_2O_3$

3. **BAP-NdEr**: $11.47Al_2O_3$-$20.51BaO$-$54.95P_2O_5$-$6.64SiO_2$-$3.83B_2O_3$-$0.5Nb_2O_3$-$1.05Nd_2O_3$ -$1.05Er_2O_3$
4. **BAP-NdYb**: $11.48Al_2O_3$-$20.52BaO$-$54.97P_2O_3$-$6.65SiO_2$-$3.83B_2O_3$-$0.5Nb_2O_3$-$1.05Nd_2O_3$-$1.0Yb_2O_3$
5. **BAP-Yb05**: $11.42Al_2O_3$-$20.41BaO$-$54.66P_2O_3$-$6.61SiO_2$-$3.80B_2O_3$-$0.5Nb_2O_3$-$1.05Nd_2O_3$-$1.05Er_2O_3$-$0.5Yb_2O_3$
6. **BAP-Yb10**: $11.36Al_2O_3$-$20.30BaO$-$54.39P_2O_3$-$6.58SiO_2$-$3.78B_2O_3$-$0.49Nb_2O_3$-$1.05Nd_2O_3$-$1.05Er_2O_3$-$1.0Yb_2O_3$
7. **BAP-Yb20**: $11.24Al_2O_3$-$20.10BaO$-$53.81P_2O_3$-$6.51SiO_2$-$3.75B_2O_3$-$0.49Nb_2O_3$-$1.05Nd_2O_3$-$1.05Er_2O_3$-$2.0Yb_2O_3$
8. **BAP-Yb30**: $11.12Al_2O_3$-$19.88BaO$-$53.27P_2O_3$-$6.44SiO_2$-$3.71B_2O_3$-$0.48Nb_2O_3$-$1.05Nd_2O_3$-$1.05Er_2O_3$-$3.0Yb_2O_3$

Reagent grade metaphosphate chemicals such as $Ba(PO_3)_2$ and $Al(PO_3)_3$ and high purity rare earth oxides, Nd_2O_3, Er_2O_3 and Yb_2O_3 with purity 99.99% from Alpha-Aesar were used as raw materials for glass preparation. Special precautions were taken in controlling the hydroxyl ion (OH^-) contents in prepared glasses by sintering the batches and maintaining the relative atmospheric humidity (RH) below 40%. Thus thoroughly mixed chemical batches were sintered at 350°C for 6 h to reduce the surface absorbed moisture and to make pre-reacted batch. Each sintered batch was then melted at 1350°C in silica crucibles for 1 h with intermittent stirrings to get homogeneity and later casted them onto preheated graphite molds. The glass samples thus obtained were kept for annealing at 550°C to relieve thermal stresses and cooled slowly to room temperature in a precise temperature controlled annealing furnace. Such annealed glasses were cut and polished in the form of plates in the dimensions of 15 x 20 x 2 mm^3 for optical characterizations.

The densities of all glasses were measured by employing the Archimedes buoyancy principle using water as buoyancy liquid. Refractive indices of glasses were

measured at five different wavelengths (473 nm, 532 nm, 632.8 nm, 1060 nm and 1552 nm) on Metricon M2010 Prism Coupler equipped with laser sources.

The UV-Vis optical absorption spectra of the Nd^{3+}, Yb^{3+}, Er^{3+} singly and co-doped barium-alumino-metaphosphate glasses were recorded on a UV-Vis spectrophotometer (Model: Lambda20, Perkin-Elmer) in the range of 200 - 1100 nm. The Fluorescence emission, excitation, and decay measurements were carried out on Fluorescence spectrophotometer (Model: Quantum Master, enhanced NIR, from Photon Technologies International) fitted with double monochromators on both excitation and emission channels. The instrument is equipped with LN_2 cooled gated NIR photo-multiplier tube (Model: NIR-PMT-R1.7, Hamamatsu) as detector for acquiring both study state spectra and phosphorescence decay. For decay measurements, a 60W Xenon flash lamp was employed as an excitation source.

Results and Discussion

Physical and optical properties

Some of the important physical and optical properties of Nd^{3+}, Yb^{3+}, Er^{3+} doped barium-alumino-metaphosphate glasses are presented in Table I. The density (d) and average molecular weight (M_{avg}) of glasses are found to be increasing with an increase in the dopant ion content due to inclusion of relatively heavy metal ions (RE^{3+}) in glass network. Using these values, Rare earth ion concentration (N_{RE}), Inter-ionic distance (r_i), Polaron radius (r_p) and Field strength (F) have been estimated using relevant relations [23, 24] and are listed out in the same table. The measured refractive indices of all Nd^{3+}, Yb^{3+},

Er^{3+} doped barium-alumino-metaphosphate glasses at 473 nm, 532 nm, 632.8 nm, 1060 nm and 1552 nm were fitted with the Sellmeire equation [25] to obtain the refractive indices at standard wavelengths, n_e (at 546.1 nm), $n_{F'}$ (at 480 nm) and $n_{C'}$ (at 643.8 nm) which have been used to calculate different optical parameters [26]. The Abbe number of all glasses is around 65 - 70 indicating the low optical dispersion in these glasses.

Spectral Properties

Optical absorption spectra

The room temperature absorption spectra of BAP-Nd, BAP-Er and BAP-Yb10 barium-alumino-metaphosphate glasses are shown in Fig. 1 as representative curves. The spectra reveal in-homogeneously broadened absorption bands due to *f-f* electronic transitions from Nd^{3+}, Yb^{3+} and Er^{3+} ions respectively. All absorption peaks have been appropriately assigned depending upon their peak energies [27]. For BAP-Nd glass doped with Nd^{3+} ions, the absorption peaks centered at 327 nm, (348 nm, 356 nm), 429 nm, 472 nm, (510 nm, 523 nm), 582 nm, 627 nm, 683 nm, 746 nm, 803 nm and 874 nm wavelengths have been detected and were assigned to transitions from ground state $^4I_{9/2}$ to the higher excited states $^4D_{7/2}$, ($^4D_{5/2}$, $^4D_{1/2}$), $^2P_{1/2}$, $^2G_{9/2}$, ($^4G_{9/2}$, $^4G_{7/2}$), ($^4G_{5/2}$, $^2G_{7/2}$), $^2H_{11/2}$, $^4F_{9/2}$, ($^4F_{7/2}$, $^4S_{3/2}$), ($^4F_{5/2}$, $^2H_{9/2}$) and $^4F_{3/2}$ respectively of Nd^{3+} $4f^3$ electronic configuration. In the case of BAP-Er glass, the absorption peaks at 364 nm, 377 nm, 405 nm, 450 nm, 487 nm, 520 nm, 545 nm, 650 nm, 802 nm and 974 nm are designated to the transitions $^4I_{15/2} \rightarrow {}^4G_{7/2}$, $^4G_{11/2}$, $^2G_{9/2}$, $^4F_{5/2}$, $^4F_{7/2}$, $^2H_{11/2}$, $^4S_{3/2}$, $^4F_{9/2}$, $^4I_{9/2}$ and $^4I_{11/2}$ of $4f^{11}$ configuration of Er^{3+} ions respectively. The absorption spectrum for BAP-Yb10 glass sample, which is triply doped with Nd^{3+}, Er^{3+} and Yb^{3+}, has exhibited respective

transitions from each dopant ion. Besides the Nd^{3+} and Er^{3+} absorption peaks, an intense absorption band at 974 nm with shoulders at 914 nm and 950 nm is due to a transition from ground state $^2F_{7/2}$ to $^2F_{5/2}$ and its corresponding stark energy levels respectively of Yb^{3+} ions [28]. From the absorption spectrum of BAP-Yb10, it has been noticed that there exists a slight increase in bandwidths of certain absorption peaks (as indexed with mixed transitions in Fig. 1) due to the absorption overlapping of different ions. From all these absorption spectra, it can be seen that absorption band due to $^4I_{9/2} \rightarrow {}^4F_{5/2}$ of Nd^{3+} at 803 nm has prominently been intense which could be availed to excite the Nd^{3+} singly and co-doped glasses for rich emissions from them.

Photoluminescence emission and excitation spectra

The room temperature photoluminescence spectra of Nd^{3+} singly, Nd^{3+}-Er^{3+} co-doped and Nd^{3+}-Yb^{3+}-Er^{3+} triply-doped barium-alumino-metaphosphate glasses obtained upon 806 nm excitation at $^4F_{5/2}$ level of Nd^{3+} ions and $^4I_{9/2}$ level of Er^{3+} are presented in Fig. 2. The emission bands centered at 887 nm, 1058 nm and 1324 nm are attributed due to transitions $^4F_{3/2} \rightarrow {}^4I_{9/2,\ 11/2\ \text{and}\ 13/2}$ respectively of Nd^{3+} and the bands at 976 nm, 1542 nm are ascribed to transitions $^2F_{5/2} \rightarrow {}^2F_{7/2}$ of Yb^{3+} and $^4I_{13/2} \rightarrow {}^4I_{15/2}$ of Er^{3+} respectively [12, 29]. All the spectra have been normalized with respect to Nd^{3+} emission at 1058 nm. The inset figure depicts a histogram representing the variation of fluorescence intensity of transition $^4F_{3/2} \rightarrow {}^4I_{11/2}$ (Nd^{3+}) and $^4I_{13/2} \rightarrow {}^4I_{15/2}$ (Er^{3+}) for different samples. It can be clearly seen that the emission intensity of Nd^{3+} decreased, while that of Er^{3+} increased on Nd^{3+}-Er^{3+} co-doping and this trend continues in the samples with the inclusion followed by successive concentration increase of Yb^{3+} ions. An enhancement of Er^{3+} emission

intensity has reached a four-fold for BAP-Yb30 sample. The increased Er^{3+} emission from co-doped samples clearly signifies the occurrence of energy transfer from Nd^{3+} to Er^{3+} in theses glasses, which increases with the increase in Yb^{3+} concentration. The mechanism involved in this energy transfer process can be understood on close examination of recorded excitation spectra for Er^{3+}, Yb^{3+} and Nd^{3+} emissions as shown in Fig. 3(a-c) respectively. Fig. 3(a) presents the excitation spectra of glasses in the wavelength range of 350 - 1000 nm by monitoring Er^{3+} emission at 1542 nm. The spectra revealed different excitation bands from all dopant Er^{3+}, Nd^{3+} and Yb^{3+} ions. The presence of both Nd^{3+} and Yb^{3+} excitation peaks in these spectra indicates their sensitization ability for Er^{3+} emission. On critical examination of these trends, it has been observed that, the excitation intensity due to both Nd^{3+} and Yb^{3+} increases with an increase in Yb^{3+} content; however, the Er^{3+} excitation intensity remains unchanged. This observed increase in the Nd^{3+} excitation intensity with an increase in Yb^{3+} concentration clearly indicates the active role played by Yb^{3+} in $Nd^{3+} \rightarrow Er^{3+}$ energy transfer.

For Nd^{3+}-Er^{3+} co-doped system, the energy transfer suggested by Shi et. al. [16] and by other authors [30] follows the mechanism (Nd^{3+}: $^4F_{3/2}$ + Er^{3+}: $^4I_{15/2}$) → (Nd^{3+}: $^4I_{15/2}$ + Er^{3+}: $^4I_{13/2}$). In the present glass host, energy difference between these transitions is found to be around 1150 cm^{-1}. This clearly implies that the energy transfer from Nd^{3+} to Er^{3+} is not resonant but involves one or more phonons. With the inclusion of Yb^{3+}, the energy transfer can occur from Nd^{3+} to Er^{3+} following the path $Nd^{3+} \rightarrow Yb^{3+} \rightarrow Er^{3+}$ as Yb^{3+} is a well-known sensitizer for Er^{3+}. The Nd^{3+} sensitization for Yb^{3+} can be evidenced from the recorded excitation spectrum by monitoring Yb^{3+} emission at 997 nm

as depicted in Fig. 3(b), which exhibited the excitation bands due to both Yb^{3+} and Nd^{3+} ions. Though the $^4I_{11/2}$ level of Er^{3+} and $^2F_{5/2}$ level of Yb^{3+} are in resonance with each other, the possibility of energy back transfer from Er^{3+} to Yb^{3+} is less owing to the quick relaxation of $^4I_{11/2}$ level of Er^{3+} to the lower level $^4I_{13/2}$ [31]. This can be realized from the absence of Er^{3+} excitation bands for Yb^{3+} emission in Fig. 3(b). The excitation spectra obtained by monitoring the Nd^{3+} emission at 1058 nm is presented in Fig. 3(c). The spectra show the excitation bands due to transitions from ground state $^4I_{9/2}$ to different excited levels of Nd^{3+} ions only. From this spectrum it is noticed that, the intensity of excitation peaks decreases with the inclusion of Er^{3+} and Yb^{3+} ions in glass matrix. This decrease in excitation intensity on co-doping with Er^{3+} and Yb^{3+} is attributed to the energy transfer from excited Nd^{3+} ions to the nearest Yb^{3+} and Er^{3+} ions. Also, there are no excitation peaks due to Yb^{3+} or Er^{3+} for Nd^{3+} emission. Thus pointing out that, even as there is an efficient energy transfer from Nd^{3+} to Yb^{3+} and in turn to Er^{3+}, no evidence of back energy transfer to Nd^{3+} from Yb^{3+} and Er^{3+} has been observed.

The emission spectra of Nd^{3+} singly-doped (BAP-Nd), Nd^{3+}-Yb^{3+} co-doped (BAP-NdYb) and Nd^{3+}-Yb^{3+}-Er^{3+} triply-doped (BAP-Yb10) barium-alumino-metaphosphate glasses in Fig. 4, gives more clear understanding on the energy transfer among these ions. For Nd^{3+} singly doped glass, the emission spectrum exhibits three distinct Nd^{3+} emission peaks at 887 nm, 1058 nm and 1324 nm of the transitions $^4F_{3/2} \rightarrow {}^4I_{9/2,\ 11/2\ \&\ 13/2}$ respectively as discussed earlier. For Nd^{3+}-Yb^{3+} co-doped glass, a strong and broad emission band due to Yb^{3+} appears at around 1 μm in addition to the three Nd^{3+} emission peaks. The emission peak at 1058 nm shows an increase in intensity for BAP-NdYb glass,

may be due to overlapping of Yb^{3+} emission stark components with it. This strong emission from Yb^{3+} upon Nd^{3+} excitation at 806 nm is due to $Nd^{3+} \rightarrow Yb^{3+}$ energy transfer in these glasses. However, on further doping with Er^{3+} (BAP-Yb10 sample), the Yb^{3+} emission intensity decreases drastically and that of Er^{3+} emission appeared at 1.54 μm. Thus, the energy transfer in the present Nd^{3+}-Yb^{3+}-Er^{3+} triply-doped barium-alumino-metaphosphate glasses follows the path $Nd^{3+} \rightarrow Yb^{3+} \rightarrow Er^{3+}$ as shown in the partial energy level diagram, Fig. 5. On excitation with 806 nm at $^4F_{5/2}$ level of Nd^{3+}, it relaxes non-radiatively to the $^4F_{3/2}$ level which then transfers the energy to Er^{3+} via Yb^{3+} in addition to the mechanism suggested by Shi et. al. [16] for $Nd^{3+} \rightarrow Er^{3+}$ direct energy transfer.

Fluorescence decay spectra

As energy transfer takes place from $^4F_{3/2}$ of Nd^{3+}, the decay analysis can be carried out with $^4F_{3/2} \rightarrow {}^4I_{9/2}$ and $^4F_{3/2} \rightarrow {}^4I_{11/2}$ transitions at 887 and 1058 nm respectively. Since $^4F_{3/2} \rightarrow {}^4I_{11/2}$ transition overlaps with Yb^{3+} emission, the transition 887 nm has been selected for decay analysis in this system. Fig. 6 shows the time resolved fluorescence spectra of Nd^{3+} emission at 887 nm. From this figure it can be seen that, the Nd^{3+} fluorescence decays rapidly on co-doping with Er^{3+} and Yb^{3+}. For Nd^{3+} singly doped sample, the decay curve is nearly single exponential with lifetime of 282 μsec. However, the exponential nature decreased with the co-doping of Er^{3+} and Yb^{3+} in these glasses. The average fluorescence lifetime (τ_{avg}) of excited level ($^4F_{3/2}$) from non-exponential decay curves of co-doped samples has been calculated using following relation [32] and the values are tabulated in Table II.

$$\tau_{avg} = \frac{\left(\frac{A1}{A2}\right)\tau_1^{\,2} + \tau_2^{\,2}}{\left(\frac{A1}{A2}\right)\tau_1 + \tau_2} \quad (1)$$

where, A1 and A2 are the weight factors of τ_1 and τ_2 respectively. From decay time values, the energy transfer rate (W_{ET}) and energy transfer efficiency (η_{ET}) have been evaluated from the following expressions [33].

$$W_{ET} = \frac{1}{\tau_{avg}} - \frac{1}{\tau_D} \quad (2)$$

$$\eta_{ET} = 1 - \frac{\tau_{avg}}{\tau_D} \quad (3)$$

where, τ_D is donor luminescence decay time in the absence of acceptor ions. The energy transfer rate is found to be increasing on co-doping with Er^{3+} and Yb^{3+} and the energy transfer efficiency of as high as 94% has been obtained for BAP-Yb30 sample, the glass containing 3 mol% of Yb_2O_3. Table II also lists the average decay times and related energy transfer parameters (W_{ET} and η_{ET}) for the emission transition $^4F_{3/2} \rightarrow {}^4I_{11/2}$ (at 1058 nm) of Nd^{3+} ions. From this table it can be seen that, 887 nm emissions show more quenching than the emission at 1058 nm.

In the case of donor-acceptor energy transfer, donor luminescence decay provides crucial information on the energy transfer micro-parameters and inter-ionic interactions responsible for energy transfer. Previous reports reveal that for Nd^{3+} to Er^{3+} energy transfer, the inter-ionic interaction cannot be a single but a mixture of interactions, which include exchange, dipole-dipole (d-d), dipole-quadrupole (d-q) and quadrupole-

quadrupole (q-q) works together [34]. Accordingly, the decay of Nd^{3+} donor luminescence for high Er^{3+} concentration shows a fast sub-microsecond decay followed by a slow non-exponential decay and an exact fit to this decay can be obtain by considering both exchange and electrostatic (d-d, d-q and q-q) interactions contributing to the energy transfer. However, for the system with low donor-acceptor concentration, the influence of short-range interactions like exchange, d-q and q-q decreases and an acceptable fit can be obtained by considering d-d interactions only. This suggests that the energy transfer interactions strongly depend on the concentration of donor and acceptor ions, particularly on the inter-ionic distances. Shi et. al. [16] demonstrated that the Nd^{3+} to Er^{3+} energy transfer is driven by d-d interactions and used F-D method but could not give a satisfactory fit to donor luminescence decay; however, Rotman et. al. [30] extended the F-D model by assuming a non-random distribution of dopants in crystal lattice and gave a good fit by considering the excluded correlation between dopants. In the present investigation, the donor decay analysis has been carried out on employing the direct energy transfer based Inokuti-Hirayama model and donor migration/diffusion assisted energy transfer based Burshtein and Yokota-Tanimoto models. Basically the energy transfer interactions between donor (Nd^{3+}) and acceptors (Yb^{3+}, Er^{3+}) in the present glass host are found to be dipole-dipole, which has been estimated from the plot of $\ln(-\ln(I(t)/I_0)-(t/\tau_0))$ versus $\ln(t/\tau_0)^3$ as shown in Fig. 7. The slope of the plot gives the value of 's' around 6, where s is the interaction parameter whose values of 6, 8 and 10 characterize for dipole-dipole, dipole-quadrupole and quadrupole-quadrupole interactions respectively [35]. By considering the dipole-dipole interactions, decay curves have been fitted with the Inokuti-Hirayama relation [36].

$$I(t) = I_0 \exp\left[-\left(\frac{t}{\tau_0}\right) - \Gamma\left(1-\frac{3}{s}\right)\left(\frac{C_A}{C_0}\right)\left(\frac{t}{\tau_0}\right)^{3/s} \right] \quad (4)$$

Where, τ_0 is the intrinsic fluorescence decay time of the donor, $\Gamma(1\text{-}3/s)$ is gamma function, C_A is acceptor ion concentration, C_0 is critical concentration defined as $(3/4\pi R_0^3)$ and s is the multipole interaction parameter (~ 6 in the present case). Fig. 8 shows the fitting curves for the experimental emission decay data at 887 nm of BAP-NdEr, BAP-Yb10 and BAP-Yb30 glasses. It is observed that, the fit obtained from Inokuti-Hirayama relation deviates from experimental data both at shorter and longer decay times. Considering the possibility of energy migration among donor ions, Burshtein's energy migration model eq. (5) and diffusion model of Yokota-Tanimoto, eq. (6) as given below have been adopted in the decay analysis [37, 38].

$$I(t) = I_0 \exp\left(-\frac{t}{\tau_0} - \gamma\sqrt{t} - Wt \right) \quad (5)$$

$$I(t) = I_0 \exp\left[-\frac{t}{\tau_0} - \frac{4\pi}{3} C_A \Gamma\left(1-\frac{3}{s}\right)(C_{DA}t)^{3/s}\left(\frac{1+10.87X+15.5X^2}{1+8.74X}\right)^{\frac{s-3}{s-2}} \right] \quad (6)$$

$$X = DC_{DA}^{-1/3}\tau_0^{2/3}$$

where, γ is energy transfer parameter, W is migration rate, C_{DA} is energy transfer micro-parameter and D is diffusion coefficient. Both Burshtein and Yokota-Tanimoto models resulted in satisfactory fits with the experimental data indicating that donor to acceptor energy transfer could be assisted through the donor-donor migration. The energy transfer

rate (γ^2), energy transfer micro-parameters (C_{DA}) and critical distance (R_0) have been derived from the fitting parameters using the relations of [39]

$$\gamma^2 = \left(\frac{C}{C_0}\right)^2 \frac{\pi}{\tau_D} \tag{7}$$

$$C_{DA} = \frac{9\gamma^2}{16 C_A{}^2 \pi^3} \tag{8}$$

$$R_0 = \left(C_{DA}\tau_0\right)^{1/6} \tag{9}$$

The calculated values have been tabulated in Table III. The energy transfer rates (γ^2) obtained using Inokuti-Hirayama model are in accordance with those calculated from measured decay times (Table II). However, for Burshtein and Yokota-Tanimoto model, the energy transfer rate is less, which is due to a fast excitation energy migration among donor ions before transfer to acceptor [40]. If the probability of donor-donor energy migration is more than donor-acceptor energy transfer, the energy transfer can be considered to be migration assisted than that of diffusion assisted. The donor-donor energy transfer micro-parameter (C_{DD}) has been calculated from the spectral overlap integral of absorption and emission cross-sections using following relation [41].

$$C_{DD} = \frac{3c}{8\pi^4 n^2} \int \sigma_{abs}^{D}(\lambda)\sigma_{em}^{D}(\lambda)d\lambda \tag{10}$$

where, c is velocity of light in vacuum, n is refractive index and $\sigma_{abs}{}^{D}(\lambda)$ and $\sigma_{em}{}^{D}(\lambda)$ are absorption and emission cross-sections of $^4F_{3/2} \leftrightarrow {}^4I_{9/2}$ transitions of Nd^{3+} ion respectively. For Nd^{3+} ions, the self-quenching is supposed to be expected through two paths. First is the cross relaxation (CR) process which involves de-population of $^4F_{3/2}$ level via following transitions: $^4F_{3/2}$:$^4I_{9/2} \rightarrow {}^4I_{15/2}$:$^4I_{15/2}$. The second process may be the resonant

energy transfer (RET) migration between the nearest neighbor excited and ground state dopant ions through $^4F_{3/2}$:$^4I_{9/2} \rightarrow {}^4I_{9/2}$:$^4F_{3/2}$ transitions. The second process is considered here to analyze the donor-donor (Nd^{3+}-Nd^{3+}) energy migration by solving eq. (10) as described above. The obtained value of energy migration micro-parameter (C_{DD}) is 3.84 x 10^{-39} cm^6sec^{-1} and the corresponding critical distance is found to be 10.3 Å. For the theoretical models adopted in present study, the donor-acceptor energy transfer micro-parameter (C_{DA}) for the Nd^{3+} singly and co-doped samples are in the order of ~10^{-42} cm^6sec^{-1} and ~10^{-40} cm^6sec^{-1} respectively which are less than the donor-donor energy migration micro-parameter (C_{DD} ~ 10^{-39} cm^6sec^{-1}). This suggests that the donor-donor energy migration is dominant over donor-acceptor energy transfer. However, the critical distance (R_0) for Nd^{3+} luminescence quenching has been increased for co-doped samples. The Nd^{3+}-Nd^{3+} critical distance of self-quenching (~3.4 Å) is very small compared to that of Nd^{3+}-Er^{3+} (~6.1 Å) and Nd^{3+}-Yb^{3+}-Er^{3+} (~6.7 Å) signifying the increase in donor-acceptor energy transfer for co-doped samples. Thus, energy transfer in the present Nd^{3+}-Yb^{3+}-Er^{3+} co-doped barium-alumino-metaphosphate glasses can be attributed to the migration assisted energy transfer.

Similarly, to have an understanding on the $Yb^{3+} \rightarrow Er^{3+}$ energy transfer, the Yb^{3+} fluorescence decay curves have also been recorded monitoring emission at 983 nm upon 806 nm excitation and are shown in Fig 9. From this figure it can be seen that, the time resolved spectrum of BAP-NdYb glass shows an initial rise followed by a slow decay with a lifetime of 1.324 ms implying the energy transfer from Nd^{3+}. In the presence of Er^{3+}, the decay curves show sharp decrease without any initial rise time, which is due to

$Yb^{3+} \rightarrow Er^{3+}$ energy transfer. Any further increase in Yb_2O_3 concentration, more quenching has been observed. Decay time falls so drastically for a glass with Yb_2O_3 above 1 mol%; this situation is due to an increased Yb^{3+}-Yb^{3+} energy migration [31]. This energy migration among Yb^{3+} ions increases the efficiency of energy transfer to Er^{3+} ions.

Conclusion

It could be concluded that a new series of barium-alumino-metaphospahte glasses single/dual/triply doped with Nd^{3+}-Yb^{3+}-Er^{3+} ions have successfully been prepared and analyzed their emission, excitation and fluorescence decay characteristics. A fourfold emission enhancement at 1542 nm of Er^{3+} has been achieved in the presence of Yb^{3+} ions while excitation through $^4I_{9/2} \rightarrow {}^4F_{5/2}$ transition of Nd^{3+} at 806 nm from barium-alumino-metaphosphate glass with 3 mol% Yb_2O_3. Emission enhancement of Er^{3+} has satisfactorily been explained based on energy transfer from Nd^{3+} to Er^{3+} through Yb^{3+} ions by the application of Inokuti-Hirayama, Burshtein (migration) and Yokota-Tanimoto (diffusion) theoretical models on the experimental decay kinetics. From the obtained results, Yb^{3+} ions are found to be providing effective bridging action between $Nd^{3+} \rightarrow Er^{3+}$ energy transfer based emission and its efficiency has been evaluated to be 94% for a NIR luminescent glass containing Nd^{3+}, Er^{3+} with 3 mol% Yb_2O_3. It has been observed that the time resolved fluorescence decay of donor ion and the energy transfer between donor and acceptor ions could be attributed to the migration assisted electrostatic dipole-dipole interactions.

Acknowledgements

Authors would like to thank Dr. H. S. Maiti, Director, CGCRI for his kind encouragement and permission to publish this work which is carried out under an In-house project No. MLP0101. Our thanks are also due to Dr. Ranjan Sen, for his kind support in the present work. One of us (Mr.A.D.S.) is thankful to the CGCRI, CSIR for the award of Research Internship to him.

References

[1] B. C. Hwang, S. Jiang, T. Luo, J. Watson, G. Sorbello, N. Peyghambarian, (2000), J. Opt. Soc. Am. B 17, 833-839.
[2] P. S. Golding, S. D. Jackson, T. A. King, M. Polnau, (2000), Phys. Rev. B. 62, 856-864.
[3] G. Sinha, A. Patra, (2009), Chem. Phys. Lett. 473, 151-154.
[4] H. Lin, X. R. Liu, E. Y. B. Pun, (2002), Opt. Mater. 18, 397-401.
[5] P. Solarz, W. Ryba-Romanowski, (2007), Radiation Measurements 42, 759-762.
[6]M. A. Noginov, M. Curley, N. Noginova, W. S. Wang, M. D. Aggarwal, (1998), Appl. Opt. 37, 5737-5742.
[7] C. Jiang, L. Jin, (2009), Appl. Opt. 48, 2220-2227.
[8] P. Tin, L. D. Schearer, (1990), J. Appl. Phys. 68, 950-953.
[9] A. B. Grudinin, S. E. Goncharov, I. D. Zalevsky, O. G. Okhotnikov, L. Gomes, N. Xiang, T. Jouhti, E. M. Dianov, I. A. ufetov, V. V. Dudin, A. V. Shubin, A. N. Guryanov, M. V. Yashkov, A. Umnikov, (2003), Opt. Soc. Am.
[10] P. R. Watekar, Seongmin Ju, Won-Taek Han, (2006), IEEE Photon. Tech. Lett, 18, 1609-1611.
[11] B. L. Davidov, A. A. Krylov, (2007), Quantum Electron. 37, 843-846.
[12] F. Liegard, J. L. Doualan, R. Moncorge, M. Bettinelli, (2005), Appl. Phys. B 80, 985-991.
[13] Y. W. Zhao, Y. F. Lin, Y. J. Chen, X. H. Gong, Z. D. Luo, Y. D. Huang, (2008), Appl. Phys. B 90, 461-464.
[14] Bor-Chyuan Hwang, Shibin Jiang, Tao Luo, Jason Watson, Gino Sorbello, and Nasser Peyghambarian, (2000), J. Opt. Soc. Am. B 17, 833-839.
[15] H. Lin, S. Jiang, J. Wu, F. Song, N. Peyghambarian, E. Y. B. Pun, (2003), J. Phys. D: Appl. Phys. 36, 812-817.
[16] W. Q. Shi, M. Bass, (1989), J. Opt. Soc. Am. B 6, 23-29.
[17] J. H. Campbel, T. I. Suratwala, (2000), J. Non-crystal. Solids 263 & 264, 318-341.
[18] Y. M. Moustafa, K El-Egili, (1998), J. non-crystal. Solids 240, 144-153.
[19] I.E.C. Machado, L. Prado, L. Gomes, J.M. Prison and J.R. Martinelli, (2004), J. Non-Crystal. Solids 348, 113-117.
[20] J. W. Fleming Jr., J. W. Shiever, (1981), United States Patent 4302074.
[21] E. T. Y. Lee, E. R. M. Taylor, (2004), J. Phys. Chem. Solids 65, 1187-1192.

[22] J. A. Capobianco, P. P. Proulx, M. Bettinelli, F. Negrisolo, (1990), Phys. Rev. B 42, 5936 – 5944.
[23] M. M. Ahmad, E. A. Hogarth and M. N. Khan, (1984), J. Mater. Sci. 19, 4041-4044.
[24] A. J. Glass laser program annual report, (1975), Lawrence-Livermore Labs. Report No. URCL-50021-72.
[25] Dieter H. Jundt, (1997), Optics Letters, Vol. 22, 1553-1555.
[26] J.H. Choi, F.G. Shi, A. Margaryan, A. Margaryan, (2005), J. Mater. Res. 20, 264-270.
[27] W. T. Carnall, P. R. Fields, K. Rajnak, (1968), J. Chem. Phys. 49, 4424-4442.
[28] G. M. Salley, R. Valiente, H. U. Gudel, (2002), J. Phys.: Condens. Matter 14, 5461-5475.
[29] J. B. Gruber, D. K. Sardar, B. Zandi, J. A. Hutchinson, C. W. Trussell, (2003), J. Appl. Phys. 93, 3137-3140.
[30] S. R. Rotman, (1990), Opt. Lett. 15, 230-232.
[31] W. Q. Shi, R. Kurtz, J. Machan, M. Bass, M. Birnbaum, M. Kokta, (1987), Appl. Phys. Lett. 51, 1218-1220.
[32] T. Fujii, K. Kodaira, O. Kawauchi, N. Tanaka, H. Yamashita, M. anpo, (1997), J. Phys. Chem. B 101, 10631-0637.
[33] G. A. Hebbink, L. Grave, L. A. Woldering, D. N. Reinhoudt, Frank C. M. J. van Veggel, (2003), J. Phys. Chem. A 107, 2483-2491.
[34] L. A. Diaz-Tores, O. Barbosa-Garcia, C. W. Struck, R. A. McFarlane, (1998), J. Lumin. 78, 69-86.
[35] J. K. Park, C. H. Kim, C. H. Han, H. D. Park, S. Y. Choi, (2003), Electrochem. Solid-State Lett. 6, H13-H15.
[36] M. Inokuti, F. Hirayama, (1965), J. Chem. Phys. 43, 1978-1989.
[37] A. I. Burshtein, (1972), Sov. Phys. JETP 35, 882-891.
[38] I. R. Martin,V. D. Rodriguez, U. R. Rodriguez-Mendoza, V. Lavin, E. Montoya, D. Jaque, (1999), J. Chem. Phys. 111, 1191-1194.
[39] L. D. da Vila, L. Gomes, L. V. G. Tarelho, S. J. L. Ribeiro, Y. Messedeq, (2003), J. Appl. Phys. 93, 3873-3880.
[40] L. D. da Vila, L. Gomes, L. V. J. Tarelho, S. J. L. Ribeiro, Y. Messaddeq, (2004), J. Appl. Phys. 95, 5451-5463.
[41] A. Braud, S. Girald, J. L. Doualan, R. Moncorge, (1998), IEEE J. Quantum Electron. 34, 2246-2255.

Figure Captions

Fig. 1: Room temperature optical absorption spectra of BAP-Nd, BAP-Er and BAP-Yb10 singly and triply-doped barium-alumino-metaphosphate glasses.

Fig. 2: Normalized luminescence spectra for singly and Nd^{3+}-Yb^{3+}-Er^{3+} co-doped barium-alumino-metaphosphate glasses with 806 nm excitation. (Inset: Histogram for Nd^{3+} and Er^{3+} emission for varying co-dopant concentrations.)

Fig. 3: Excitation spectra of Nd^{3+}-Yb^{3+}-Er^{3+} triply-doped barium-alumino-metaphosphate glasses upon monitoring the Er^{3+} emission at 1542 nm (a), Yb^{3+} emission at 997 nm (b) and Nd^{3+} emission at 1058 nm (c).

Fig. 4: Normalized emission spectra of BAP-Nd, BAP-NdYb and BAP-Yb10 glasses.

Fig. 5: Partial energy level diagram for the energy transfer mechanism from Nd^{3+}, Yb^{3+} and Er^{3+} doped in barium-alumino-metaphosphate glasses.

Fig. 6: Decay curves of Nd^{3+} emission at 887 nm excited at 806 nm. Solid lines are the theoretical fits using Burshtein donor energy migration model.

Fig. 7: Plots of experimental decay data $\ln(t/\tau_0)^3$ vs. $\ln[-\ln(I(t)/I_0)-(t/\tau_0)]$ of Nd^{3+} emission at 887 nm with the solid lines represent linear fits to the data points.

Fig. 8: Experimental decay curves of 887 nm emissions of BAP-NdEr, BAP-Yb10 and BAP-Yb30 glasses with the theoretical fits using inokuti-Hirayama, Burshtein and Yokota-Tanimoto models respectively.

Fig. 9: Decay curves of Yb^{3+} emission at 976 nm with λ_{ex} = 806 nm. Solid lines are the exponential fits to data points used for lifetime calculation

Table I: Important physical and optical properties; density (d), average molecular weight (M_{avg}), molar volume (V_M), concentration of dopant ions (N_{RE} in 10^{20} ions/cm^3), inter-ionic distance (r_i), polaron radius (r_p), field strength (F), refractive index (n_e, $n_{F'}$ and $n_{C'}$), Abbe number (ν_e) and reflection loss (R%) of different Nd^{3+}, Yb^{3+}, Er^{3+} doped barium-alumino-metaphosphate glasses.

Glass	BAP-Nd	BAP-Er	BAP-NdEr	BAP-Yb0.5	BAP-Yb1	BAP-Yb2	BAP-Yb3
Physical Properties							
d (g/cm^3)	3.037	3.033	3.060	3.095	3.101	3.150	3.184
M_{avg} (g/mol)	134.1	134.5	136.7	138.0	139.3	142.0	144.6
V_M (cm^3)	44.1	44.4	44.6	44.6	44.9	45.1	45.4
N_{Nd}	2.88	-	2.844	2.835	2.824	2.820	2.799
N_{Er}	-	2.865	2.844	2.835	2.824	2.820	2.799
N_{Yb}	-	-	-	1.353	2.677	5.345	7.960
r_i (Å)	15.14	15.17	12.07	11.25	10.63	9.69	9.03
r_p (Å)	6.10	6.11	4.86	4.53	4.28	3.91	3.64
F (10^{14} cm^{-2})	8.06	8.03	12.68	14.59	16.34	19.66	22.63
Optical Properties							
n_e	1.5529	1.5512	1.5532	1.5534	1.5546	1.5554	1.5559
$n_{F'}$	1.5567	1.5549	1.5571	1.5574	1.5587	1.5595	1.5601
$n_{C'}$	1.5488	1.5471	1.5491	1.5493	1.5504	1.5512	1.5516
ν_e	70.0	70.6	69.3	68.7	67.2	66.9	65.4
R%	4.69	4.67	4.69	4.70	4.71	4.72	4.73

Table II: Measured fluorescence lifetime (τ_{avg}), Energy transfer rate (W_{ET}) and Energy transfer efficiency (η_{ET}) derived from decay of Nd^{3+} emission at 1058 nm and 887 nm on 806 nm excitation.

Glass	**$^4F_{3/2} \rightarrow {}^4I_{11/2}$ (1058 nm)**			**$^4F_{3/2} \rightarrow {}^4I_{9/2}$ (887 nm)**		
	τ_{avg} (μsec)	**W_{ET} (sec^{-1})**	**η_{ET} (%)**	**τ_{avg} (μsec)**	**W_{ET} (sec^{-1})**	**η_{ET} (%)**
BAP-Nd	287.4	-	-	282.0	-	-
BAP-NdEr	198.1	1567	31.1	154.2	2939	45.3
BAP-Yb05	92.8	7292	67.7	36.5	23851	87.0
BAP-Yb10	79.9	9042	72.2	27.9	32296	90.1
BAP-Yb20	36.5	23917	87.3	21.3	43402	92.4
BAP-Yb30	22.9	40209	92.1	16.4	57429	94.2

Table III: The experimental values of Energy transfer parameter (γ), Transfer rate (γ^2), Critical concentration (C_0), Energy transfer micro-parameter (C_{DA}), Critical distance (R_0), Migration rate (W) and Diffusion coefficient (D) obtained from different models for Nd^{3+} emission decay at 887 nm in barium-alumino-metaphosphate glasses on 806 nm excitation.

Glass	γ ($sec^{-1/2}$)	γ^2 (sec^{-1})	C_0 (10^{20} ions/cm^3)	C_{DA} (10^{-40} cm^6sec^{-1})	R_0 (Å)	W (sec^{-1})	D (10^{-11} cm^2sec^{-1})
Inokuti-Hirayama (eq. 4)							
BAP-Nd	4.73	22.38	60.7	0.049	3.4	-	-
BAP-NdEr	38.40	1474.9	7.38	3.31	6.8	-	-
BAP-Yb05	91.01	8282.5	4.59	8.57	8.0	-	-
BAP-Yb10	105.57	11145.82	5.19	6.68	7.7	-	-
BAP-Yb20	175.19	30690.8	4.65	8.35	8.0	-	-
BAP-Yb30	231.96	53805.7	4.62	8.43	8.0	-	-
Burshtein (eq. 5)							
BAP-Nd	4.72	22.56	60.45	0.049	3.4	0.543	-
BAP-NdEr	26.92	724.68	10.53	1.62	6.1	830	-
BAP-Yb05	60.18	3621.43	6.94	3.74	7.0	2820	-
BAP-Yb10	67.20	4515.84	8.16	2.71	6.6	3790	-
BAP-Yb20	101.99	10401.96	7.98	2.83	6.7	9570	-
BAP-Yb30	110.10	12166.09	9.72	1.91	6.3	21980	-
Yokota-Tanimoto (eq. 6)							
BAP-Nd	4.73	22.37	60.71	0.049	3.4	-	-
BAP-NdEr	29.14	849.14	9.73	1.905	6.2	-	0.40
BAP-Yb05	65.72	4319.12	6.35	4.467	7.2	-	0.91
BAP-Yb10	73.93	5465.64	7.42	3.277	6.9	-	1.01
BAP-Yb20	113.84	12958.54	7.15	3.526	6.9	-	1.94
BAP-Yb30	114.47	13103.38	9.37	2.054	6.4	-	4.45

Spectral Overlap (eq. 10)

Glass	C_0 (10^{20} ions/cm^3)	C_{DD} (10^{-40} cm^6sec^{-1})	R_0 (Å)
BAP-Nd	2.12	38.4	10.3

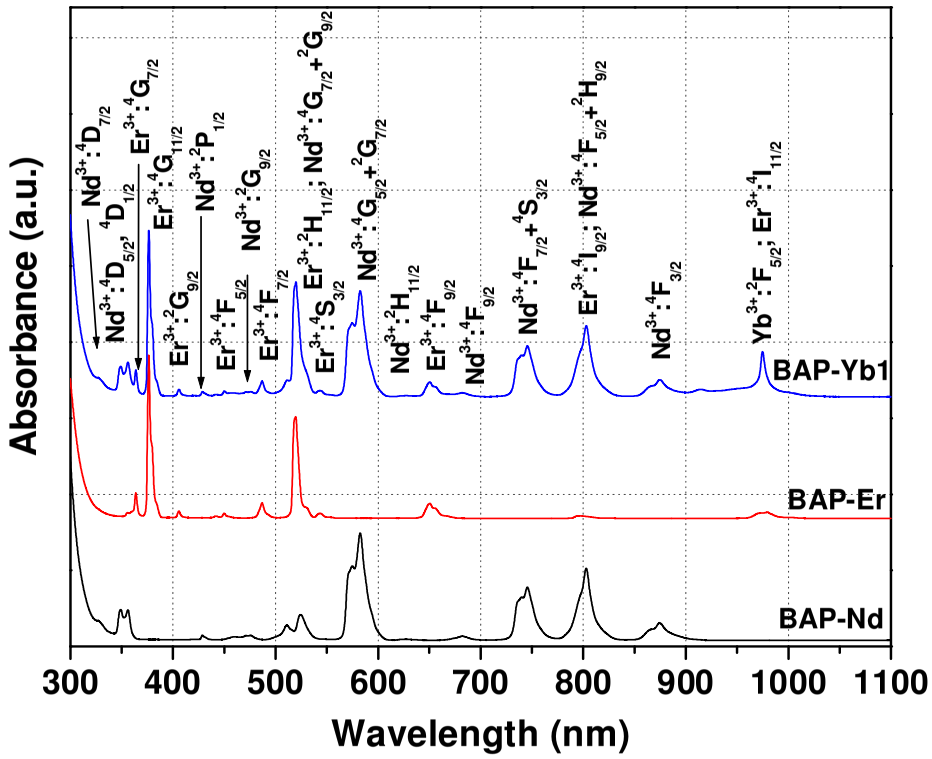
Absorbance (a.u.)
Wavelength (nm)
300
400
500
600
700
800
900
1000
1100
BAP-Yb1
BAP-Er
BAP-Nd
Nd3+:4D7/2
Nd3+:4D5/2, 4D1/2
Er3+:4G7/2
Er3+:4G11/2
Er3+:2G9/2
Nd3+:2P1/2
Er3+:4F5/2
Nd3+:2G9/2
Er3+:4F7/2
Er3+:4S3/2
Er3+:2H11/2; Nd3+:4G7/2+2G9/2
Nd3+:4G5/2+2G7/2
Nd3+:2H11/2
Er3+:4F9/2
Nd3+:4F9/2
Nd3+:4F7/2+4S3/2
Er3+:4I9/2; Nd3+:4F5/2+2H9/2
Nd3+:4F3/2
Yb3+:2F5/2; Er3+:4I11/2

Fig. **1**

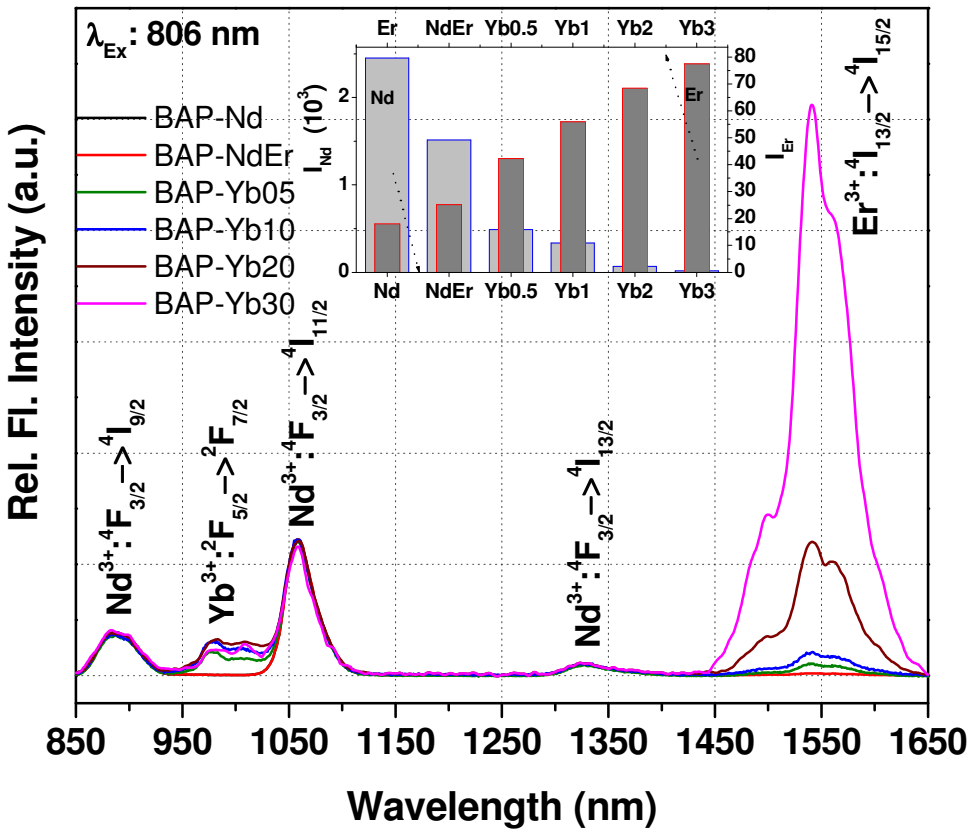
λEx: 806 nm
BAP-Nd
BAP-NdEr
BAP-Yb05
BAP-Yb10
BAP-Yb20
BAP-Yb30
Rel. Fl. Intensity (a.u.)
Wavelength (nm)
850
950
1050
1150
1250
1350
1450
1550
1650
Nd3+:4F3/2 –> 4I9/2
Yb3+:2F5/2 –> 2F7/2
Nd3+:4F3/2 –> 4I11/2
Nd3+:4F3/2 –> 4I13/2
Er3+:4I13/2 –> 4I15/2
Er
NdEr
Yb0.5
Yb1
Yb2
Yb3
Nd
INd (10^3)
IEr

Fig. 2

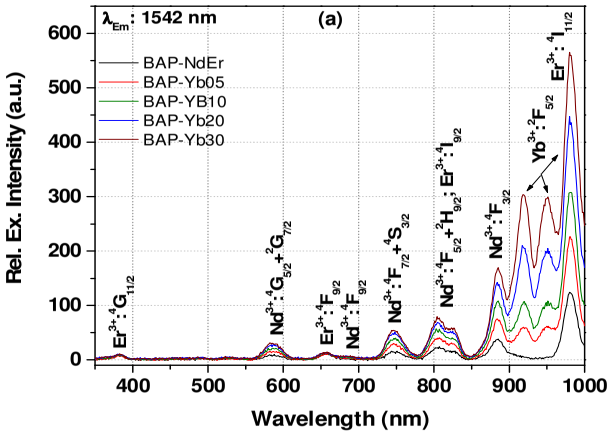
λEm: 1542 nm
(a)
BAP-NdEr
BAP-Yb05
BAP-YB10
BAP-Yb20
BAP-Yb30
Rel. Ex. Intensity (a.u.)
Wavelength (nm)
Er3+:4G11/2
Nd3+:4G5/2+2G7/2
Er3+:4F9/2
Nd3+:4F9/2
Nd3+:4F7/2+4S3/2
Nd3+:4F5/2+2H9/2; Er3+:4I9/2
Nd3+:4F3/2
Yb3+:2F5/2
Er3+:4I11/2

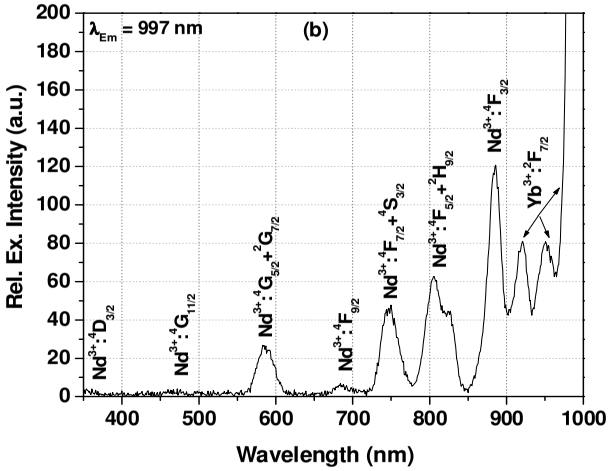
λEm = 997 nm
(b)
Rel. Ex. Intensity (a.u.)
Wavelength (nm)
Nd3+:4D3/2
Nd3+:4G11/2
Nd3+:4G5/2+2G7/2
Nd3+:4F9/2
Nd3+:4F7/2+4S3/2
Nd3+:4F5/2+2H9/2
Nd3+:4F3/2
Yb3+:2F7/2

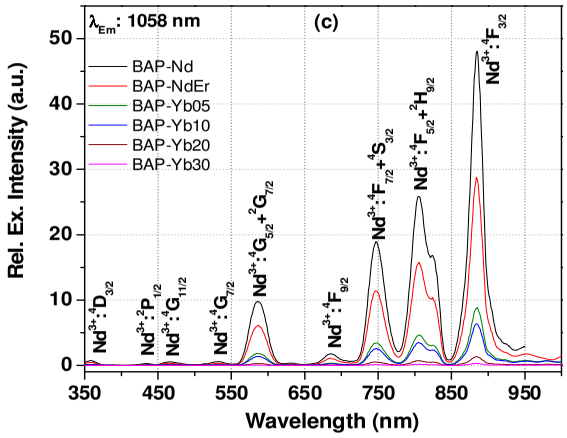
λEm: 1058 nm
(c)
BAP-Nd
BAP-NdEr
BAP-Yb05
BAP-Yb10
BAP-Yb20
BAP-Yb30
Rel. Ex. Intensity (a.u.)
Wavelength (nm)
Nd3+:4D3/2
Nd3+:2P1/2
Nd3+:4G11/2
Nd3+:4G7/2
Nd3+:4G5/2+2G7/2
Nd3+:4F9/2
Nd3+:4F7/2+4S3/2
Nd3+:4F5/2+2H9/2
Nd3+:4F3/2

Fig. 3

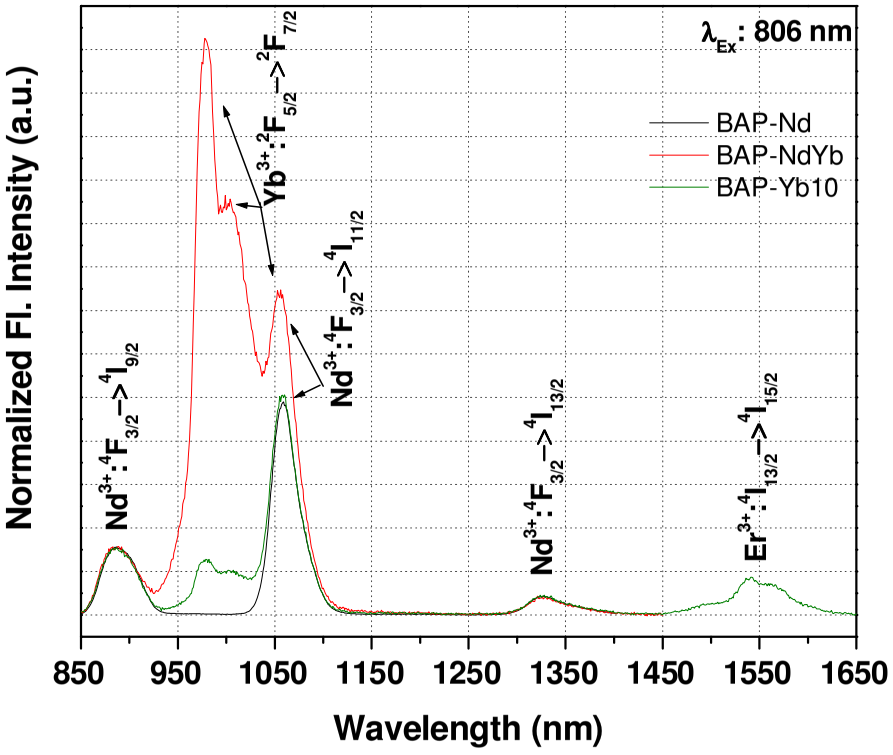
λEx: 806 nm
BAP-Nd
BAP-NdYb
BAP-Yb10
Normalized Fl. Intensity (a.u.)
Wavelength (nm)
850
950
1050
1150
1250
1350
1450
1550
1650
Nd3+:4F3/2 –> 4I9/2
Yb3+:2F5/2 –> 2F7/2
Nd3+:4F3/2 –> 4I11/2
Nd3+:4F3/2 –> 4I13/2
Er3+:4I13/2 –> 4I15/2

Fig. 4

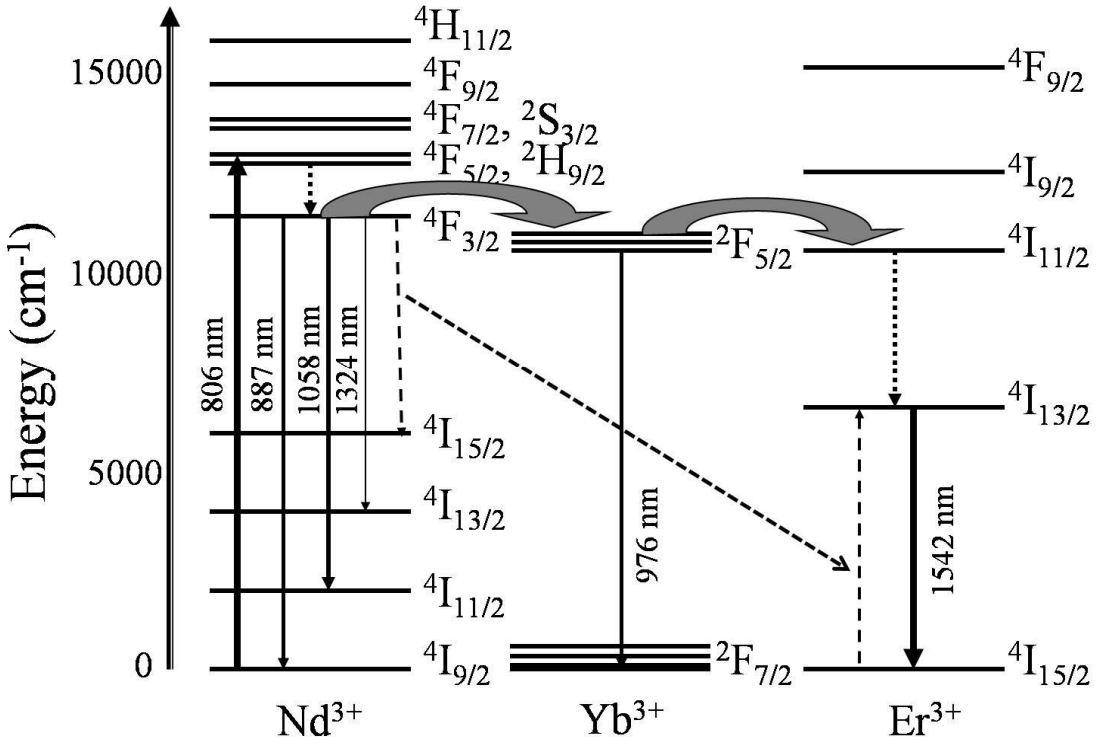
Energy (cm-1)
15000
10000
5000
0
4H11/2
4F9/2
4F7/2, 2S3/2
4F5/2, 2H9/2
4F3/2
4I15/2
4I13/2
4I11/2
4I9/2
2F5/2
2F7/2
4F9/2
4I9/2
4I11/2
4I13/2
4I15/2
806 nm
887 nm
1058 nm
1324 nm
976 nm
1542 nm
Nd3+
Yb3+
Er3+

Fig. 5

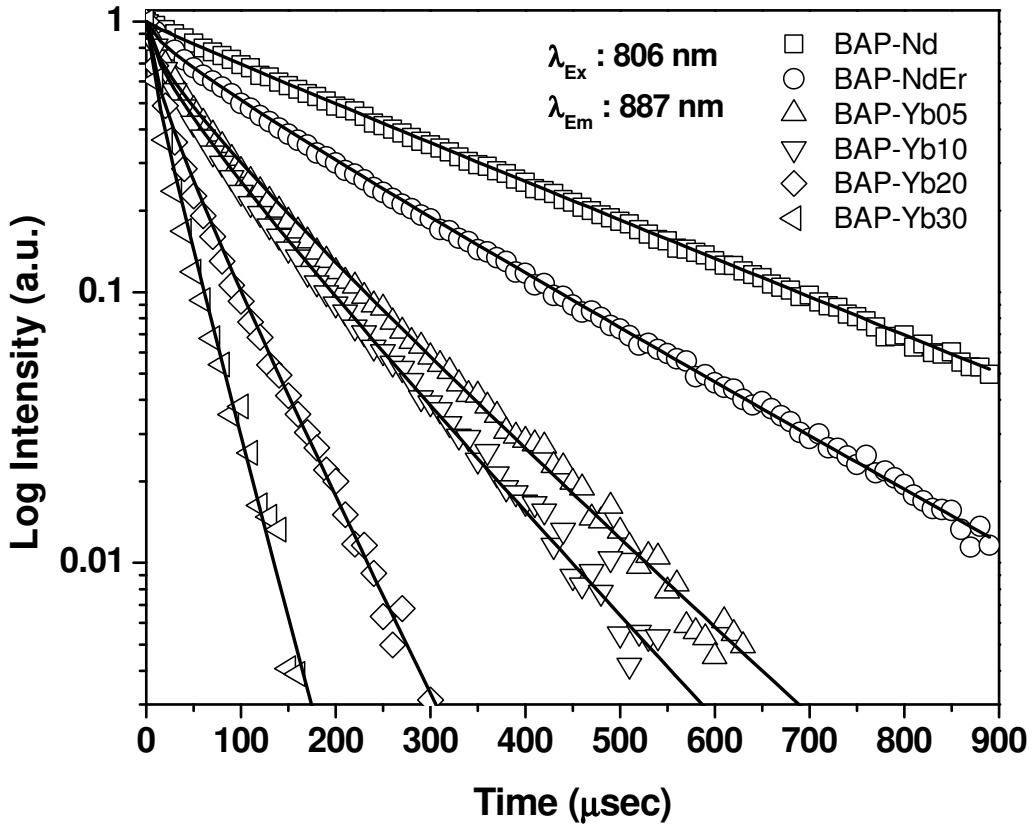
1
0.1
0.01
Log Intensity (a.u.)
0
100
200
300
400
500
600
700
800
900
Time (μsec)
λEx : 806 nm
λEm : 887 nm
BAP-Nd
BAP-NdEr
BAP-Yb05
BAP-Yb10
BAP-Yb20
BAP-Yb30

Fig. 6

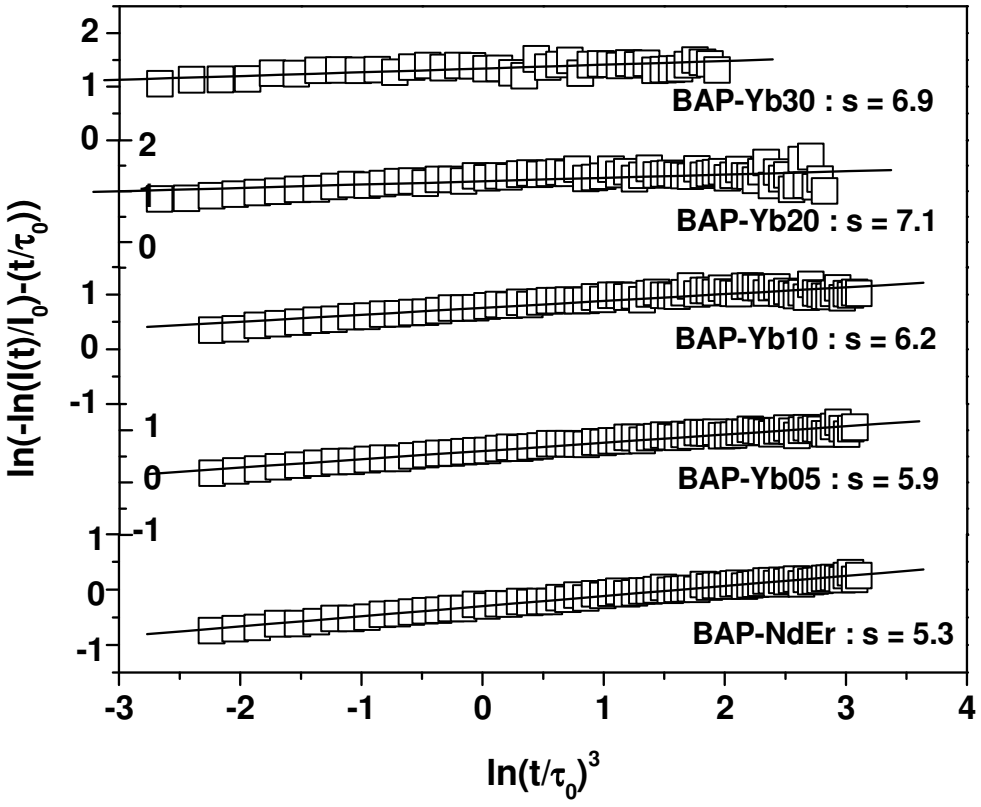
BAP-Yb30 : s = 6.9
BAP-Yb20 : s = 7.1
BAP-Yb10 : s = 6.2
BAP-Yb05 : s = 5.9
BAP-NdEr : s = 5.3
ln(-ln(I(t)/I0)-(t/τ0))
ln(t/τ0)3

Fig. 7

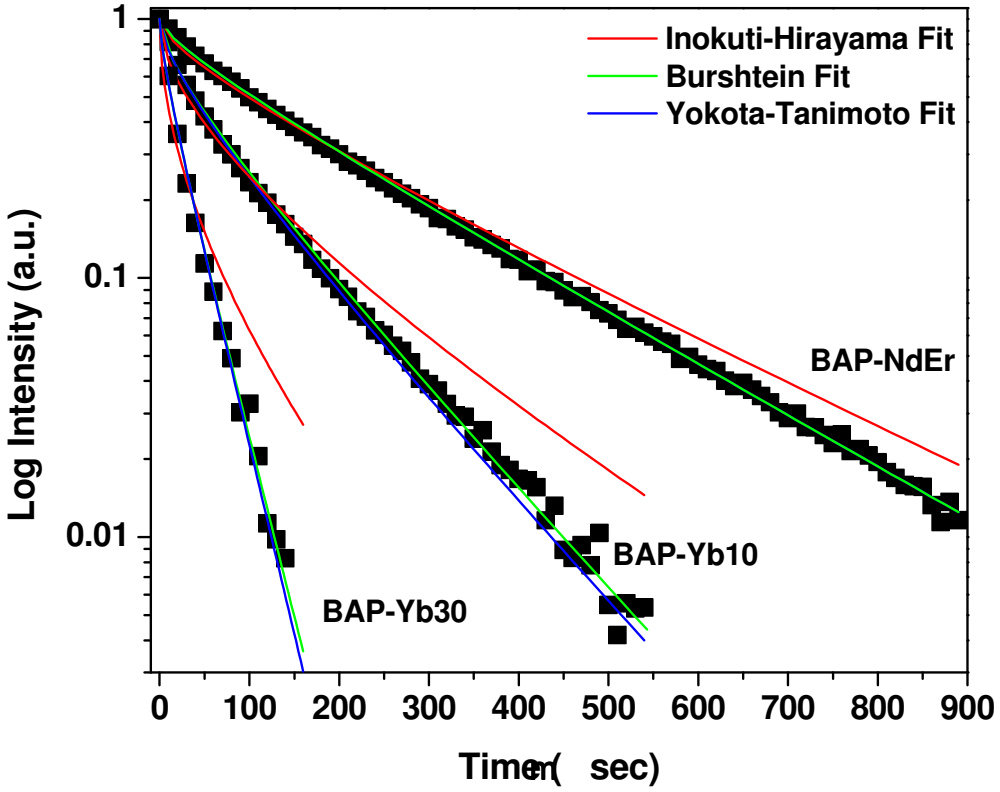
Inokuti-Hirayama Fit
Burshtein Fit
Yokota-Tanimoto Fit
BAP-NdEr
BAP-Yb10
BAP-Yb30
Log Intensity (a.u.)
Time (sec)
1
0.1
0.01
0
100
200
300
400
500
600
700
800
900

Fig. 8

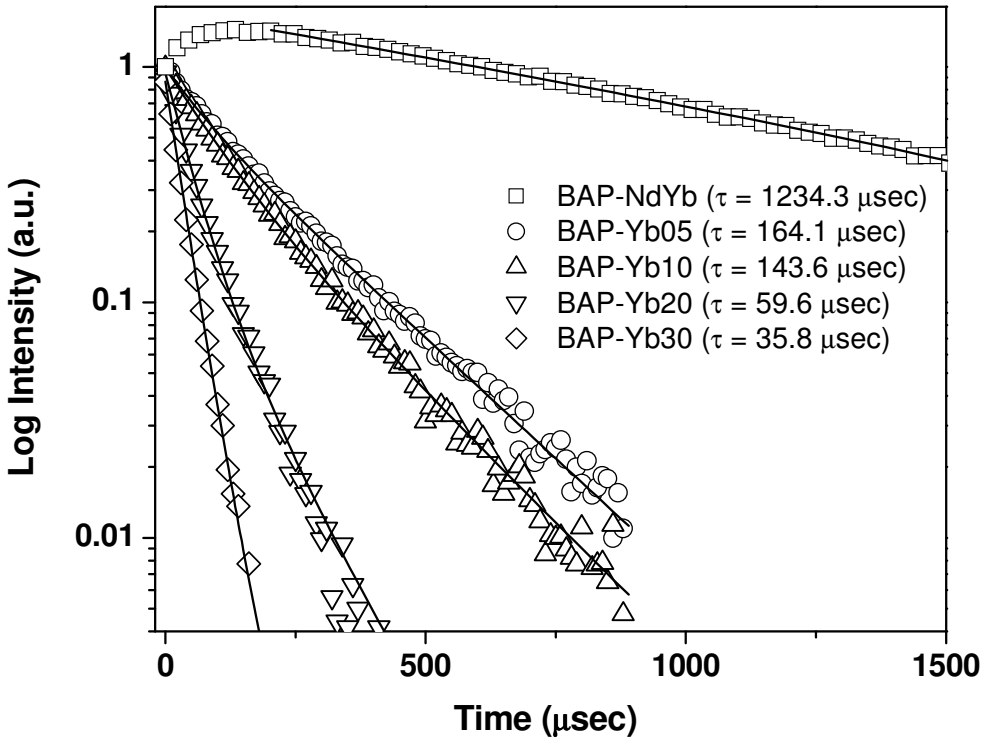
Log Intensity (a.u.)
1
0.1
0.01
0
500
1000
1500
Time (μsec)
BAP-NdYb (τ = 1234.3 μsec)
BAP-Yb05 (τ = 164.1 μsec)
BAP-Yb10 (τ = 143.6 μsec)
BAP-Yb20 (τ = 59.6 μsec)
BAP-Yb30 (τ = 35.8 μsec)

Fig. 9